

Measuring Shapes of Galaxy Images II: Morphology of 2MASS Galaxies

Nurur Rahman and Sergei F. Shandarin

Department of Physics and Astronomy, University of Kansas, Lawrence, KS 66045, USA;
nurur@kusmos.phsx.ukans.edu, sergei@ku.edu

ABSTRACT

We study a sample of 112 galaxies of various Hubble types imaged in the Two Micron All Sky Survey (2MASS) in the Near-Infra Red (NIR; 1–2 μm) J , H , and K_s bands. The sample contains (optically classified) 32 elliptical, 16 lenticulars, and 64 spirals acquired from the 2MASS Extended Source Catalogue. We use a set of non-parametric shape measures constructed from the Minkowski Functionals (MFs) for galaxy shape analysis.

We use ellipticity (ϵ) and orientation angle (Φ) as shape diagnostics. With these parameters as functions of area within the isophotal contour, we note that the NIR elliptical galaxies with $\epsilon > 0.2$ show a trend of being centrally spherical and increasingly flattened towards the edge, a trend similar to images in optical wavelengths. The highly flattened elliptical galaxies show strong change in ellipticity between the center and the edge. The lenticular galaxies show morphological properties resembling either ellipticals or disk galaxies. Our analysis shows that almost half of the spiral galaxies appear to have bar like features while the rest are likely to be non-barred. Our results also indicate that almost one-third of spiral galaxies have optically hidden bars.

The isophotal twist noted in the orientations of elliptical galaxies decreases with the flattening of these galaxies indicating that twist and flattening are also anti-correlated in the NIR, as found in optical wavelengths. The orientations of NIR lenticular and spiral galaxies show a wide range of twists.

Key words: galaxies: morphology - galaxies: structure - galaxies: statistics

1 INTRODUCTION

Galaxy morphology in different wave-bands provides useful information on the nature of galaxy evolution as well as the overall distribution of galaxy constituents such as old red giants, young luminous stars, gas, dust etc. For example, the younger Population I stars associated with massive gas-rich star formation regions light up the disk galaxies in optical wavelengths. The distribution of older Population II stars, the dominant matter component near the central regions of galaxies, remains hidden. The presence of interstellar dust hides the old stellar population especially in late-type disk galaxies. The NIR light, on the other hand, is much less affected by the interstellar dust and more sensitive to the older populations. Thus it provides a penetrating view of the core regions in disk galaxies. Therefore careful analysis of morphological differences between the optical and infrared images would not only provide valuable insight into the role of population classes in morphology but also reveal whether the discrepancies are due to singular or combined effects of extinction and population differences (Jarrett et al. 2003).

In the morphological studies of cosmological objects the

most widely used technique is the ellipse-fitting method, (Carter 1978; Williams & Schwarzschild 1979; Leach 1981; Lauer 1985; Jedrzejewski 1987; Fasano & Bonoli 1989; Franx, Illingworth & Heckman 1989; Peletier et al. 1990). In this study we use a set of measures known as the Minkowski functionals (hereafter MFs, Minkowski 1903) to analyze the morphology of NIR galaxies. Contrary to the conventional method, the MFs provide a non-parametric description of the images implying that no prior assumptions are made about the shapes of the images. The analyses based on the MFs appear to be robust and numerically efficient when applied to various cosmological studies, e. g., galaxies, galaxy-clusters, CMB maps etc. (Mecke, Buchert & Wagner 1994; Schmalzing & Buchert 1997; Kerscher et al. 1997; Schmalzing & Gorsky 1998; Hobson, Jones & Lasenby 1999; Novikov, Feldman & Shandarin 1999; Schmalzing et al. 1999; Beisbart 2000; Kerscher et al. 2000a; Novikov, Schmalzing, & Mukhanov 2000; Beisbart, Buchert & Wagner 2001a; Beisbart, Valdarnini & Buchert 2001b; Kerscher et al. 2001b; Shandarin 2002; Shandarin et al. 2002; Sheth et al. 2003; Rahman & Shandarin 2003, hereafter paper 1)

This is the second in a series of papers aimed to study the morphology of galaxy images using a set of measures derived from the MFs. In this paper we analyze a larger sample of 2MASS galaxies imaged at J , H , and K_s band in NIR (Jarrett 2000; Jarrett et al. 2000; Jarrett et al. 2003). We have described and tested the set of Minkowski parameters derived from the two-dimensional scalar, vector and several tensor MFs to quantify galaxy shapes for a small sample of 2MASS images in paper I. The analyses in paper I used contour smoothing to reduce the effect of background noise. We have used the same technique in the present sample which contains NIR galaxies over the entire range of Hubble types including ellipticals, lenticulars and spirals. The present investigation is aimed at obtaining structural information on 2MASS galaxies by measuring their shapes quantified by ellipticity and orientation. As dusty regions of galaxies become transparent in the NIR, the imaging in this part of the spectrum should provide a clear view of the central core/bulge regions of these objects. A systematic study of NIR images should provide valuable information regarding the central structures of galaxies (e. g., optically hidden bar) which would otherwise remain absent when viewed in optical wavelengths. If only the old red giants illuminate galaxies at NIR wavelengths and are decoupled from Population I star lights, then the NIR galaxies should show weak isophotal twist in their orientations compared to those in the visual wavelengths. Therefore it would be interesting to check whether or not isophotal twist is a wavelength dependent effect.

The organization of the paper is as follows: the 2MASS sample and selection criteria are described in §2, a brief discussion of the parameters is given in §3. We discuss the robustness of the measures to identify and discern galaxy isophotes of various shapes and present our results §4. We summarize our conclusions in §5. In the appendix (§6) we demonstrate the sensitivity of several Minkowski measures to image contamination by foreground stars.

2 2MASS DATA

The 2MASS catalogue contains near-infrared images of nearby galaxies within redshift range from $cz \sim 10,000$ km s⁻¹ to 30,000 km s⁻¹. The survey utilizes the NIR band windows of $J(1.11 - 1.36 \mu\text{m})$, $H(1.50 - 1.80 \mu\text{m})$ and $K_s(2.00 - 2.32 \mu\text{m})$. The 2MASS images have 1'' pixel resolution and 2'' beam resolution. The seeing FWHM values for these images are typically between 2.5'' and 3'' in all three bands. For details of the 2MASS observations, data reduction and analysis, readers are referred to Jarrett (2000) and Jarrett et al. (2000, 2003).

Our sample contains 112 galaxies imaged in NIR J , H , and K_s bands. It includes 32 elliptical, 16 lenticulars, and 64 spirals acquired from the 2MASS Extended Source Catalogue (XSC; Jarrett et al. 2003). The spiral sample contains 19 normal (SA), 21 transitional (SAB), and 24 barred (SB) galaxies. The galaxy types are taken from the RC3 catalogue (de Vaucouleurs et al. 1992). The sensitivity and resolution ($\sim 2''$) of the NIR data obtained in the 2MASS is not adequate to derive independent galaxy sub-classification (Jarrett 2000), therefore, we rely on the morphological clas-

sification based upon optical data derived in combination with both imaging and spectroscopy.

We construct the sample by hand with a moderately large number of galaxies of each type to make statistical inferences. The primary motivation behind constructing the sample is to make a comparative analysis with previous results and to investigate the galaxies with new tools to gain further insight into overall galaxy morphology in infrared wave-bands. We consider only bright galaxies in three different bands; the K_s band total magnitude for the galaxies is $7 \leq K_s \leq 12$. Spiral galaxies with inclination up to $i \sim 60^\circ$ are included in the sample. No deprojection has been made to any of these galaxies prior to the analysis since the projection effect does not pose a serious threat to the reliability of the analysis when using a parameter such as ellipticity in the structural analysis of low inclination spiral galaxies (Martin 1995; Abraham et al. 1999).

All galaxies in our sample are flat fielded and background subtracted. Except for three ellipticals, foreground stars have been removed from the rest of the sample. Those galaxies where a foreground star is left embedded in images are included purposely to illustrate the sensitivity of the morphological measures, as explained in the appendix.

3 MINKOWSKI FUNCTIONALS AS SHAPE DESCRIPTORS

For an object with arbitrary shape a complete morphological description requires both topological and geometrical characteristics. The MFs consist of a set of measures carrying both geometric (e. g., area, perimeter) and topological (the Euler Characteristic, EC) information about an object. The functionals obey a set of properties such as motion invariance, additivity and continuity (see Schmalzing 1999; Beisbart 2000). For this study we derive morphological parameters using a selection of two-dimensional scalar, vector, and tensor MFs as described in paper I.

We treat every image as a set of contour lines corresponding to a set of surface brightness levels. A contour is constructed by linear interpolation at a given level. For every contour, the first step of the functional analysis provides three scalars: A_S , P_S , and EC (also represented by the symbol, χ); three vectors or centroids: A_i , P_i , and χ_i ; and a total of nine components of three symmetric tensors A_{ij} , P_{ij} , and χ_{ij} . Here $i, j = 1, 2$ (for details see paper 1). In the next step, the eigenvalues (λ_1 and λ_2 ; $\lambda_1 > \lambda_2$) of the tensors are found taking centroids as the origins of corresponding tensors. After calculating the eigenvalues, we proceed to construct the axes and orientations of the ‘‘auxiliary ellipse’’ (hereafter AE). To construct the area tensor AE, for example, we take the eigenvalues of A_{ij} and ask what possible ellipse may have exactly the same tensor. When we find that particular ellipse, we label it as the area tensor AE. The orientation of the semi-major axis of the AE with respect to the positive x-axis is taken as its orientation. The AEs corresponding to the perimeter and EC tensors are constructed in a similar manner. To discern morphologically different objects, therefore, we use ellipticities (ϵ_i) and orientations (Φ_i) of the AEs rather than the eigenvalues of the tensors. We define ellipticity of the AEs as

$$\epsilon_i = 1 - b_i/a_i,$$

where i corresponds to one of the three tensors, and a and b are the semi-major and semi-minor axes of the AEs.

The use of AEs effectively relates a contour to an ellipse: the similarity of three AEs is a strong evidence that the shape of the contour is elliptical. For example, in case of a perfect elliptic contour, the AEs will be the same. In particular, the areas of all three AEs will be equal to the area of the contour, i. e., $A_A = A_P = A_\chi = A_S$, and the perimeters of the ellipses will be equal to the perimeter of the contour, i. e., $P_A = P_P = P_\chi = P_S$. In addition, the orientations of all three ellipses will coincide with the orientation of the contour. Therefore, if plotted, all three AEs will be on top of each other, overlapping with the contour. For that contour, all three vector centroids will also coincide with each other and with the center of the contour. Note that the latter alone does not guarantee that the contour itself is elliptical in nature since for any centrally symmetric contour the centroids would coincide. However, for a non-elliptical contour all three AEs will be different in size and orientation (see Fig. 1, paper I).

Note that the sets of eigenvalues from three tensors can be used to construct three ‘‘anisotropy’’ parameters instead of three AEs (see also Beisbart 2000). The parameters can be defined as

$$\mathcal{A}_i = \frac{\lambda_{1,i} - \lambda_{2,i}}{\lambda_{1,i} + \lambda_{2,i}},$$

where i has the same meaning as before. To better understand the behaviors of ϵ_i and \mathcal{A}_i , we show these parameters in Fig. 1 as functions of contour area (A_S) for four elliptic profiles of different flattening. Panel 1 of the figure shows ellipticity for all four profiles. Panels 2, 3, and 4 show, respectively, \mathcal{A}_A , \mathcal{A}_P , and \mathcal{A}_χ where each of these panels also has four profiles. For each profile, we find that the ϵ_i of the AEs are identical and coincide with each other (panel 1). The \mathcal{A}_i , on the other hand, do not coincide even for perfect elliptic contours (panels 2, 3, and 4). We also find that the relative separations between different \mathcal{A}_i change with the flattening of the contours. From the behavior of the parameters one can think that the ϵ_i of the AEs act as parameters that are scaled with respect to the \mathcal{A}_i . For contours with arbitrary flattening, the \mathcal{A}_i from the area and EC tensors need to scale down to match with the ϵ_i of the respective AEs. The \mathcal{A} from the perimeter tensor, however, needs to scale up for spherical and moderately elongated contours. For highly elongated contours, however, all three \mathcal{A} s need to scale down.

The illustration of the ‘‘anisotropy’’ parameter serves two purposes. First, it gives us a feeling of the AEs compared to the conventional parameter that deals with eigenvalues. Second, it demonstrates that one can derive various shape measures from the set of MFs. Apart from this parameter, one can also derive the shapefinder statistic as suggested by Sahni, Sathyaprakash & Shandarin (1998). However, we restrict ourselves to ellipticity and orientation since these are the two widely used measures in astronomy. We will explore the sensitivity and robustness of \mathcal{A}_i in our future work on optical galaxies.

The non-parametric approach for shape analysis, such as moments technique, has been known to the astronomical community for some time (Carter 1978; Carter & Metcalf 1980). It should be mentioned here that the morphological

analyses based only on the moments of inertia would provide incomplete and sometimes misleading results. As an example, let us assume that one has a galaxy image which has been kept in a black box and analyzed using simply the inertia tensor without having a priori knowledge of the shape of the image. The analysis based only on the moments of inertia will provide a resultant ellipticity of the object regardless of its actual shape. Using this result one can always infer an elliptical shape for the unseen object. If one raises the question of the likeliness of the elliptical shape of the object, the analysis based on the inertia tensor alone will not be able to give a satisfactory answer. One needs to invoke additional measure(s) in order to justify the result. It is at this point where the measures derived from the set of MFs appear to be effective. Subsequent analyses of the image using moments of the perimeter and EC tensor enables one to pin down the type of the galaxy and thus ensures the objectivity of the analysis.

The ellipticities obtained from different AEs provide information (regarding shapes) similar to the conventional shape measure based on inertia tensor. The main difference is that the conventional method finds the eigenvalue of the inertia tensor for an annular region enclosing mass density or surface brightness. The method based on MFs, however, finds the eigenvalues of contour(s) where the region enclosed by the contour(s) is assumed to be homogeneous and to have constant surface density.

In order to reduce the effect of noise present in the image we use a simple smoothing technique. Instead of smoothing the whole image, we smooth contours at each brightness level using the procedure known as the unequally weighted moving average method. The goal of this smoothing is to restore the initial unperturbed contour as much as possible and measure its morphological properties. The implementation of the smoothing is described in detail in paper I.

Contour smoothing considerably improves the estimates of ellipticity derived from the tensor functionals (see Figs. 8 and 9, paper I), therefore, in this study, we focus on the results obtained only from the smoothed contours. However, we note two effects that arise as a result of smoothing. First, in the outer regions of galaxies a smoothed, outer contour crosses the inner one. It happens occasionally; however, the area within the smoothed, outer contour remains greater than the inner one and does not affect the measurement. Second, in case of very large contour, we lose information. The smoothing technique is an iterative process depending on the number of points along a contour (see paper 1 for details). A highly irregular contour that consists of large number of points eventually shrinks to a point due to excessive smoothing. As a result we do not get any contribution from it. However, this does not pose any threat on getting relevant information of the shape of image contours since we can always compare with the unsmoothed profiles to see how much information is lost.

4 RESULTS

In this paper we use a different notation to express ellipticity than in paper I where we used $E = 10*(1-b/a)$ in the range 0 to 10. The symbol E for the ellipticity parameter is often used for the definition of the Hubble types for ellipticals

and this symbol and range can be misleading when used as a parameter for other types of galaxies (e. g., spirals). We, therefore, use ϵ_i as the characteristic of shape with the range 0 to 1.

The ellipticity and orientation can be used to isolate galaxies into two broad bins: non-barred and barred systems. For finer distinction we need to use other parameters such as luminosity, color, surface brightness, half-light radius, etc. Both of these parameters have been applied to quantify properties of elliptical galaxies (e.g. Carter 1978; Williams & Schwarzschild 1979; Leach 1981, Lauer 1985; Jedrzejewski 1987; Fasano & Bonoli 1989; Franx, Illingworth & Heckman 1989; Peletier et al. 1990). In many recent works this set of parameters has been used to obtain information on different structural components, e. g., bar, bulge, disk etc. of disk galaxies (Athanasoula et al. 1990; Martin 1995; Wozniak et al. 1995; Rozas, Knapen & Beckman 1998; Abraham & Merrifield 2000; Laurikainen, Salo & Rautainen 2002; Peng et al. 2002, Erwin & Sparke 1999; Erwin & Sparke 2003; Michel-Dansac & Wozniak 2004).

Galaxies with different morphologies appear to show characteristic signatures in the ellipticity profile. For example, the profile of elliptical galaxies is generally monotonic. A barred galaxy, however, shows a distinct peak with a spherical central region, signaling the presence of a central bulge and a bar. On the other hand, for a multi-barred system several peaks appear in the profile (Wozniak et al. 1995; Erwin & Sparke 1999).

Elliptical galaxies usually show twists (i. e., a change in the orientation of AE) in the orientation profiles with varied strength depending on the flattening of the contours. Barred galaxies, on the other hand, not only have large twists in their orientations but also have characteristic features such as a sharp peak, or two different but approximately constant orientations with an abrupt change in between (Wozniak et al. 1995; Erwin & Sparke 1999).

In the contemporary studies, therefore, a barred galaxy is identified as the system whose ellipticity and orientation profile simultaneously show the distinctive signatures mentioned above. In this study we follow the same criterion to analyze disk galaxies, i. e., we identify bars by visual inspection with the condition that both ellipticity and orientation profiles show the characteristic features simultaneously. However, identifying disk galaxies as barred systems with the above criterion (as used in previous studies mostly in optical wavelengths) should be used with caution. Our experience shows that optically classified barred galaxies appear with distinct peaks in their ellipticity profiles but show continuous orientation over the region where the peak in the shape profiles persists. Therefore we feel that more elaborate treatment is needed for identifying barred systems rather than simply relying on the behaviors of ellipticity and orientation. In this study, therefore, when we encounter these types of systems, we refrain from drawing any conclusions about these galaxies. We will explore the detailed shape properties of these galaxies in our future study including other structural measures such as Fourier decomposition technique (Quillen, Frogel & Gonzalez 1994; Buta & Block 2001).

We measure ellipticity and orientation for a set of contours obtained at different surface brightness levels. Gener-

ally these two parameters vary with the area of the contour, i. e., $\epsilon_i = \epsilon_i(A_S)$ and $\Phi_i = \Phi_i(A_S)$.

We analyze each galaxy at 30 different brightness levels where the levels correspond to equally spaced areas on a logarithmic scale covering almost the entire region of each galaxy. At every brightness level, contours are found and subsequently smoothed. All three AEs are constructed from the smoothed contours. In order to reduce information content we present our final results using only the area tensor AE and hence drop the subscript i . Below we briefly discuss the justification of the choice. For each galaxy, therefore, we show ϵ and Φ of this particular AE as a function of contour area (A_S).

For each galaxy, a thick dashed line is used to show the mean values of ϵ and Φ calculated from J, H , and K_s bands. The mean values are used to estimate the overall change ($\Delta\epsilon$ and $\Delta\Phi$) which is defined as the difference between the highest and lowest value of the corresponding mean value. It is a single number and independent of A_S . Two thin solid lines are used to show the maximum and minimum of the measures obtained from different bands. The difference between these two thin solid lines is used to quantify the scatter ($\delta\epsilon$ and $\delta\Phi$) in the parameters. The δ varies at different regions of a galaxy and so depends on A_S . We use it as an indicator to measure the dependence of galaxy shapes on different colors.

For each sample of galaxies, the result is presented in increasing order of 2MASS ellipticity obtained from the 2MASS catalogue. The 2MASS ellipticity and orientation are measured for the $3 \times \sigma_n$ isophote in the K_s band (σ_n is the rms amplitude of the background noise provided by the catalogue). For each galaxy, the 2MASS shape parameter is, therefore, a single number. Our analysis, on the other hand, provides a range of values obtained at different regions (recall that ϵ or Φ is a function of area) from the galactic center. We use the 2MASS estimate of ellipticity and position angle as the reference. It is shown by the horizontal dashed line. In all plots the vertical dashed line represents the contour area (A_S) corresponding to K_s band $3 \times \sigma_n$ isophote. We rescale the orientation profiles of a few galaxies to fit the desired ranges that have been chosen to show the Φ profiles.

Note that our results presented below correspond to the area $\log_{10} A_S \geq 1.5$. The range is chosen in order to exclude discreteness effects due to the grid. The deviation (Δ) as well as the scatter (δ) in the parameters, therefore, will be considered in this range.

4.1 Shape of Isopotential Contour and The Role of Tensor Ellipses

From section §3 we know that for a perfect elliptic contour, the areas enclosed by the AEs will be the same whereas for non-elliptic contours they will be different. Therefore, comparing the areas enclosed by different ellipses one can probe to which extent the shape of a contour can be approximated by an ellipse.

Galaxies appear more regular in NIR wave bands than in the visual wavelengths. For example, a galaxy may appear grand in the visual bands with its giant spiral arms. However, it will lose much of its grandeur in infrared wavebands. Since spiral arms consist mostly of gas and young bright stars, they will be absent in long wavelength parts of

the spectrum. To see up to what extent galaxy contours of different Hubble types retain their characteristic signatures in NIR and how tensor ellipses help us to understand their shapes, we draw readers attention to Figs. 2 and 3. In these figures we show the relative difference in areas enclosed by three different AEs as a function of contour area (A_S) for a selection of elliptical and spiral galaxies. The figures highlight only the interesting parts along the vertical axis. Each panel contains a total of nine curves: three curves corresponding to three AEs from each band. The dark, medium and light colors represent, respectively, the J , H , and K_s band. We show the area, perimeter, and EC ellipses, respectively, by the solid, dotted, and dashed-dotted lines.

Apart from three galaxies that are marked by “S”, the isophotal contours of most of the galaxies in Fig. 2 show elliptic nature in the NIR. Few of these, e. g., NGC 3158 and NGC 2778 (galaxy number 8 and 15 respectively) appear slightly non-elliptic in one or two bands. The galaxies marked by “S” (number 1, 4, and 7) are galaxies which have foreground stars embedded in their image. For these galaxies the notable feature is the sharp increase in area around the region of the images where the star is embedded. One can see that the same ellipse overlaps in different bands. This is most notable from the EC ellipse (dashed-dotted line) since the EC tensor is the most sensitive to any disturbance along the contour. The other two ellipses also behave in a similar manner but with less sensitivity. This particular behavior shows that the AEs detect unusual features attached to otherwise perfectly elliptical image body. For example, when we compare NGC 3158 or NGC 2778 with those three galaxies, we notice that A_χ not only differs in different bands but it also spreads out differently around the edge. It tells us that the contours of these galaxies are simply non-elliptic around the edge without any abnormal feature.

When we compare galaxies of different Hubble types, we find that almost all spiral galaxies (Fig. 3) show more non-elliptic nature than the elliptical galaxies. The non-elliptic nature of spiral galaxy isophotes is reflected strongly in the behavior of the EC ellipse in all bands. For these galaxies, the EC ellipse is different not only from other two ellipses but it is also spread out arbitrarily in different bands.

From Figs. 2 and 3, it is clear that all three AEs are useful for better characterization of a galaxy image. The information provided by the AEs definitely help to get finer distinction of galaxies. Since our current interest is to focus on the gross morphological features rather than looking at the finer details of galaxy isophotes, to reduce the information content, therefore, we will only use the area tensor AE to present our final results.

4.2 Ellipticals

The sample of elliptical galaxies has been divided into two groups. Group 1 contains galaxies with small ellipticities ($\epsilon \leq 0.2$) while Group 2 has galaxies with $\epsilon > 0.2$. To simply locate a galaxy within a group, we label them with an integer number. For example, NGC 4374(2) means that NGC 4374 is the second galaxy in its relevant group. In each group galaxy number 1 has the lowest 2MASS ellipticity whereas number 16 has the highest value. We follow the same format for all types of galaxies. Note that below we highlight only those galaxies that have interesting/unusual morphological

features. The general trends of galaxies will be investigated in §5.

Group 1

Ellipticity: The ellipticity profiles of galaxies in this group are shown in Fig. 4. NGC 4374(2) and NGC 4261(9), have uncommon profiles compared to other galaxies. These galaxies are more elongated in the region $1.8 < \log_{10} A_S < 3.0$ than either around the center or near the edge which makes their profiles look “centrally arched” (marked by “A”). This particular type of behavior is shown only by sphericals and is absent in elongated galaxies.

The following three galaxies are shown with an “S” mark in Fig. 4: NGC 4278(1), NGC 3193(4), and NGC 3379(7). These galaxies have sharp kinks in the ϵ profiles. These sharp changes are caused by a foreground star and do not correspond to any structural feature (see appendix). The rest of the galaxies show profiles typical of ellipticals. Galaxies in this group, in general, have small scatter.

Orientation: The orientation profiles of galaxies are presented in Fig. 5. NGC 4458(3) is stable from the center up to $\log_{10} A_S \approx 2.8$ and shows a large deviation near the edge. NGC 3193(4) shows a notable peak in its orientation. Its profile shows a dip around the region where the foreground star is embedded. NGC 3379(7) does not show any unusual feature in its profile. Its position angle, as well as the scatter, gradually increases towards the galactic center. NGC 3379(7) has larger scatter at all distances from the galactic center than NGC 4278(1) and NGC 3193(4).

Note that the presence of a star on the galaxy contours may or may not be detected by the Φ profile. The ϵ profile, on the other hand, is sensitive to any kind of disturbance on the contour. If the unusual feature on the contour attributed by the star happens to be along the major axis, which is the case for NGC 3379(7), it remains unnoticed and no peak appears in the Φ profile. This is the reason why the presence of a star on the contours may be missed as a signature on the Φ profile. On the other hand, if the feature is slightly off the major axis, it changes the orientation of the contour significantly with respect to the inner and outer contours. This is the case for NGC 4278(1) and NGC 3193(4).

In spite of being a spherical galaxy (E1+), NGC 4494(6) has remarkably low twist ($\Delta\Phi \sim 3.5^\circ$) and scatter in its orientation. It is very unusual because a spherical contour is highly susceptible to background noise. A slight perturbation caused by the noise distorts the contour’s shape and the direction of perturbation becomes its orientation.

VCC 1737(10), NGC 3159(12), and NGC 3226(13) have orientation profiles quite similar to disk galaxies as shown later in this section. The Φ profiles of VCC 1737(10) and NGC 3226(13) appear “arch like” where the latter galaxy has a longer arch than the former. These three galaxies also have large scatter in their orientations.

Group 2

Ellipticity: The ellipticity profiles of galaxies in this group are shown in Fig. 6. Galaxies with $\epsilon > 0.2$ show a “centrally spherical” trend in their profiles. The variation in the profile becomes stronger with the increasing flattening of the galaxies. The overall change in ϵ observed from the center to the edge varies from galaxy to galaxy. It changes

from as low as ~ 0.12 (NGC 315(2)) to as high as ~ 0.33 (NGC 5791(15)).

The measurements for most of the galaxies in all three bands nicely coincide. As a result the galaxies in this group show the lowest amount of scatter.

Orientation: The orientation profiles of galaxies in this group are shown in Fig. 7. The flattened ellipticals have quite stable orientations with relatively low twist and scatter compared to those in group 1. For all galaxies the $\Delta\Phi$ is within 10° .

The relatively small twist observed in the elliptical galaxies with $\epsilon > 0.2$ suggests that flattening and isophotal twists are most likely anti-correlated in the NIR wave-bands (see §6 and Fig. 18 for more). This result is in agreement with the (optical) correlation found by Galletta (1980) who noted that the maximum apparent flattening and the highest observed twist are inversely related.

4.3 Lenticulars

The sample of lenticulars contains 16 galaxies. The ellipticity and orientation of these galaxies are shown in Figs. 8 and 9 respectively.

Ellipticity: For NGC 1315(1), our estimate indicates a spherical inner part ($\epsilon \sim 0.05$) in between $1.2 \leq \log_{10} A_S \leq 2.6$, suggesting a spherical bulge for the galaxy. NGC 3598(7), IC 4064(8), NGC 3816(12), NGC 3768(13), and NGC 2577(16) have profiles quite similar to elliptical galaxies: a smoothed variation in elongation with radius.

Orientation: The orientations of lenticular galaxies generally have larger scatter than the elliptical galaxies. NGC 4659(4) shows the largest twist in this sample, ($\Delta\Phi \sim 68^\circ$); its orientation experiences a large change within $1.5 \leq \log_{10} A_S \leq 2.3$.

Lenticular galaxies with (2MASS) ellipticity $\epsilon > 0.30$ (from galaxy number 8 and above in Fig. 9) are observed to have less scatter than their spherical counterparts. This property is quite similar to flattened ellipticals. The scatter is large for lenticulars that are spherical in shape and it varies at different regions from the galaxy centers.

- Both shape and orientation profiles of NGC 4620(9) and NGC 2544(14) exhibit a bar like feature. These galaxies are labeled as “IB” where “IB” stands for “infrared bar”.

4.4 Spirals

The sample of spirals has been divided into four groups based on the degree of scatter ($\delta\epsilon$) observed in the ϵ profiles. $\delta\epsilon$ is measured for all A_S in the range $\log_{10} A_S \geq 1.5$. Group 1 contains spirals that have the least scatter while group 4 has galaxies with the largest scatter. Galaxies with $\delta\epsilon \leq 0.05$ are included into group 1, for group 2 the range is $0.05 < \delta\epsilon \leq 0.1$, those with $0.1 < \delta\epsilon \leq 0.2$ are in group 3, and finally galaxies with $\delta\epsilon > 0.2$ define group 4. The grouping of the spiral sample has been done by visual examination of the ellipticity profiles and therefore it is quite crude; our intention is simply to highlight the interesting features apparent in the shape profiles of spiral galaxies viewed in the NIR. In these groups, galaxies are organized by increasing order of (2MASS) ellipticity.

Group 1

Ellipticity: The ellipticity profiles of galaxies in this group are shown in Fig. 10. Only four galaxies are optically classified (RC3) as barred systems. These are NGC 4262(2), NGC 4024(3), NGC 3384(10), and NGC 4394(13). Except the last one, the shape profiles of other three galaxies possess distinctive feature, i. e., a clear appearance of peak(s) in the profiles, indicating (qualitatively) similar morphology both in optical and NIR. These three galaxies are labeled as “OIB” where “OIB” stands for “optical and infrared bar”. We label NGC 4394(13) as “OB” where “OB” stands for “optical bar” only. We give our explanation below for this labeling.

NGC 4151(6) is a highly spherical galaxy compared to other members of this group. It has $\epsilon < 0.05$ from the galactic center up to $\log_{10} A_S \approx 3.2$; beyond this limit the ellipticity increases a little bit. This galaxy, an intermediate ringed transitional spiral, is most likely dominated by a very large spherical bulge. The profiles of IC 3831(8), NGC 4143(9), NGC 3418(11), and NGC 5326(12) are quite similar to elliptical galaxies.

NGC 3912(15) and UGC 5739(16) are two highly flattened galaxies in this group. Their profiles appear “centrally arched”, an unusual feature shown by several NIR elliptical galaxies.

Orientation: The orientation profiles of galaxies in this group are presented in Fig. 11. The overall twists ($\Delta\Phi$) in these galaxies range in between $\sim 5^\circ - 55^\circ$.

NGC 4151(6), a galaxy of spherical shape, shows the largest scatter in its orientation. Since highly spherical contours can be perturbed easily by noise, it is not surprising that the galaxy would have large variations in its orientation at different wave-bands. The profile of NGC 4143(9) is quite similar to the barred galaxy NGC 3384(10), although its orientation changes smoothly compared to that of NGC 3384(10).

- The profiles of NGC 3177(4) and NGC 3684(5) show a bar like feature although these galaxies are optically classified as non-barred systems. However, we label these galaxies as “IB” after careful visual inspection of their unsmoothed and smoothed profiles.

The profiles of NGC 4651(7) and NGC 4494(13) deserve attention because of their complex morphologies. The ellipticity profile of NGC 4651(7) has a peak that is confined within $2.5 < \log_{10} A_S < 3.0$. In this region its orientation is different from the bulge and the disk. Since it is an early type spiral with *rs* subclass, we think the feature is due to the ring. According to RC3 classification NGC 4494(13) is a barred galaxy. But from the NIR profile it is not clear whether the galaxy really possesses a bar like structure. The galaxy is devoid of any distinct peak in its shape profile even though it has considerable amount of twist ($\Delta\Phi \sim 32^\circ$). It shows higher flattening near the edge which is probably the elongation of the disk. We are uncertain about the actual shape and therefore label the galaxy as “OB” (optical bar).

Group 2

Ellipticity: The ellipticity profiles of galaxies in this group are shown in Fig. 12. It contains seven galaxies that are optically classified as barred systems. The galaxies are NGC 3974(1), IC 357(7), NGC 4662(10), NGC 6347(11), NGC 5737(13), UGC 2585(14), and IC 568(16). These galaxies show a bar like feature in their NIR ellipticity profiles.

We, therefore, label them as “OIB”. The profiles of NGC 3277(2) and NGC 4714(8) are quite similar to elliptical galaxies.

Orientation: The orientation profiles of the galaxies in this group are shown in Fig. 13. The overall twists range between $\sim 5^\circ - 71^\circ$. The profiles of NGC 3974(1) and IC 357(7) have similar characteristics: a constant direction along the central bars while the orientation changes in the central bulge and outside disk.

- The following three galaxies are optically-classified non-barred spirals: NGC 4146(3), IC 863(6), and UGC 5903(9). However, these galaxies show bar like features in their NIR profiles and therefore we label them as “IB”.

Note that the orientation profile of NGC 4152(4) has two distinct peaks. Its ellipticity profile, however, does not possess any feature to be considered as a barred galaxy. Therefore we are not certain whether or not it can be considered as a barred galaxy.

The orientation profile of NGC 5478(12) shows two different directions. Its shape changes considerably around the region where the position angle changes. The variation in ellipticity is extended over a wide region. From visual inspection a question can be raised about whether or not the galaxy is a barred system. A careful inspection of both unsmoothed and smoothed profiles indicates that it is not a barred galaxy.

Group 3

Ellipticity: The ellipticity profiles of galaxies in this group are shown in Fig. 14. This group contains the largest number of optically classified barred galaxies: NGC 5716(3), UGC 3936(4), NGC 4375(6), UGC 7073(9), NGC 3811(11), IC 742(12), NGC 5260(13), IC 1764(15), and UGC 3839(16). Except for NGC 4375(6) and UGC 7073(9), the NIR profiles of other 7 galaxies show similarity (at least qualitatively) with their optical morphology (“OIB”). The profiles of both NGC 4375(6) and UGC 7073(9) lack characteristic signatures in their profiles and therefore have been labeled as “OB”.

Orientation: The orientations of galaxies are shown in Fig. 15. The overall twists range between $\sim 10^\circ - 71^\circ$. The twist as well as scatter in the orientations of these galaxies are high compared to those in the previous two groups.

Among “OIB” galaxies, only UGC 3936(4) and UGC 3839(16) have large twists in their orientations. For other “OIB” galaxies, the twists are relatively small.

- The following three galaxies are optically classified as non-barred spirals: UGC 2303(1), UGC 3053(2), and NGC 3618(8). The profiles of these galaxies in NIR, however, show features similar to barred systems. We label these galaxies as “IB” after visual inspection of their unsmoothed and smoothed profiles.

Group 4

Ellipticity: The ellipticity profiles of galaxies in this group are shown in Fig. 16. According to RC3 catalogue, the following four galaxies are barred systems: UGC 2705(4), UGC 3171(9), NGC 5510(13), and UGC 1478(16). It is interesting to note that the NIR profiles of none of these galaxies have characteristic features resembling bar like systems. Therefore we label these galaxies as “OB”.

Orientation: The orientations of galaxies in spiral group 4 are shown in Fig. 17. The overall twists range between $\sim 15^\circ - 70^\circ$. Galaxies in this group have the highest scatter in their orientations compared to those in the other three groups.

Among “OB” galaxies, UGC 1478(16) has a unique profile. The galaxy has a distinct, highly flattened, central bar. Its orientation is constant along the central bar and changes sharply to the orientation of the disk.

- The following three galaxies are optically-classified non-barred systems: NGC 1219(1), UGC 3091(8), and UGC 7071(11). The NIR profiles of these galaxies, however, show features similar to barred galaxies (“IB”). These spirals generally have larger twists compared to the “OB” galaxies.

4.5 Comparison with the 2MASS Estimate

We use shape parameters estimated by the 2MASS as the reference. Our analysis should provide estimates similar to the 2MASS for contours enclosing larger areas. Since $3 \times \sigma_n$ isophote corresponds to a low surface brightness level, i. e., a region near the edge of a galaxy image, we would expect agreement only in this region.

For the purpose of comparison with we use only the relative error between the shape of the contour closest to K_s band $3 \times \sigma_n$ isophote and the 2MASS estimate. In most cases we find excellent agreement (within $\sim 10\%$ of the 2MASS). However, in a few cases the agreement is poor (beyond $\sim 10\%$ of the 2MASS) and in this section we report only these cases.

We want to stress that the result presented here is obtained after careful comparison of both unsmoothed and smoothed profiles of the parameters. We do not include galaxies whose unsmoothed profiles agree with the 2MASS (i. e., within $\sim 10\%$ of the 2MASS). For example, we do not include NGC 4394 (13, spiral group 2; Fig. 12) in the list of galaxies given below since its unsmoothed profile shows excellent agreement with the 2MASS. The apparent mismatch between the 2MASS and our estimate for smoothed profile is due to the effect of smoothing (as mentioned in §3). If the unsmoothed profile of a galaxy shows disagreement (i. e., beyond $\sim 10\%$ of the 2MASS) in the first place, it is also reflected in its smoothed profile and only then we include the galaxy in the list. For these galaxies, therefore, the estimates of the parameters from both unsmoothed and smoothed profiles disagree with the 2MASS. We note that that an agreement in the ϵ profile a galaxy does not necessarily mean that it will also have an agreement in its Φ profile.

Note particularly that for several elliptical galaxies we do not have any contour near the $3 \times \sigma_n$ level. We do not attempt to make any comparison for these galaxies.

Ellipticity: The difference in the estimate of ellipticity is seen only for lenticular and spiral galaxies. The galaxies showing the difference comprise $\sim 32\%$ of the entire sample. Here we provide the list of these galaxies: 11, 14 in Fig. 4; 5, 16 in Fig. 6; 1, 3, 6, 8, 9, 11, and 15 in Fig. 8; 1, 6, 8, 14, and 16 in Fig. 10; 1, 7, 13, 14, and 16 in Fig. 12; 3, 4, 8, 11, 13, 14, 15, and 16 in Fig. 14; 2, 6, 11, 13, 14, 15, and 16 in Fig. 16.

Orientation: The difference in the estimate of orientation appears in all types of galaxies. For the following

galaxies ($\sim 23\%$ of the entire sample) we have found disagreement: 3, 8, 10, and 13 in Fig. 5; 6, 8, and 9 in Fig. 9; 2, 6 and 14 in Fig. 11; 1, 7, 10, 13, 14, and 16 in Fig. 13; 1, 8, 13, and 15 in Fig. 15; 1, 4, 8, 9, 11, and 15 in Fig. 17. For these galaxies our estimate of Φ is either lower or higher than the 2MASS.

We want to point out that while for some galaxies (e. g., 3 and 8 in Fig. 4) the estimates of ϵ are in agreement with 2MASS, the estimates of Φ for these galaxies (3 and 8 in Fig. 5) differ. In some cases our analyses do not reach the $3 \times \sigma_n$ isophote level (e. g., 3 and 8 in Fig. 4; 8 and 9 in Fig. 8; 6 in Fig. 10; 7 in Fig. 12) which is a likely reason for disagreement.

We draw reader's attention to galaxies numbered 11 and 14 in Fig. 4 and listed above. The ϵ and Φ profiles of these galaxies may give an impression to the reader that they do not reach the $3 \times \sigma_n$ level (recall that the figures showing these profiles are for smoothed contours). In fact they do reach the level for the unsmoothed profiles and disagree with the 2MASS. This particular appearance of the profiles arise due to excessive smoothing at the outer part of these galaxies (see §3).

We provide analyses for smoothed isophotes. Contour smoothing can be thought of as a method to minimize the effect of noise to restore the original shape. Since the 2MASS results have not been estimated from smoothed isophotes, we want to emphasize that there is no guarantee that the shape estimates provided by the survey represent the actual shape of galaxy contours. After careful comparison of both unsmoothed and smoothed profiles of galaxies, we feel reasonably confident that the disagreement is not entirely due to the methodological difference. It is likely that our approach is better capable of revealing the actual shapes of galaxy isophotes, especially around the edge.

5 CONCLUSIONS

We have analyzed a sample of galaxies of various Hubble types obtained from the 2MASS catalogue. The sample contain 112 galaxies imaged in the NIR J , H , and K_s bands. We have used ellipticity (ϵ) and orientation angle (Φ), as functions of area within the isophotal contour, as the diagnostic of galaxy shape. These measures have been constructed from a set of non-parametric shape descriptors known as the Minkowski Functionals (MFs). The ellipticity and orientation for each galaxy have been derived at 30 different surface brightness levels in each of these bands. The ellipticity and position angle (for K_s band only) provided by the 2MASS are used as the reference in our analysis.

Our results show that the elliptical galaxies with $\epsilon \geq 0.2$ appear to be centrally spherical. These galaxies show smooth variations in ellipticity with the size, quantified by the area within the contour, and are more flattened near the edge than the central region. A variation as strong as $\Delta\epsilon \geq 0.25$, from the center towards the edge, is noticeable in more flattened systems, e. g., NGC 4125, NGC 3377, NGC 4008, and NGC 5791 (9, 10, 12, and 15 in group 2 of elliptical galaxies; Fig. 6). This behavior is similar to previous studies of ellipticals in visual bands (Jedrzejewski 1987, Fasano & Bonoli 1989, Franx et al. 1989). The similarity in apparent shapes in optical and NIR wavelengths indicates that the low

ellipticity noticed at the central regions of these galaxies is intrinsic rather than an artifact contributed by the seeing effect. Additionally the ϵ profiles of these galaxies appear very similar in different NIR bands with a very low scatter. This suggests that the morphological differences that are likely to appear in different bands are weak in NIR elliptical galaxies.

The twist ($\Delta\Phi$), characterized by the overall change in the orientation with radius, observed in the orientations of elliptical galaxies decreases with increasing flattening. A relatively small twist shown by ellipticals with $\epsilon > 0.2$ suggests that elongation and isophotal twist are likely to be anti-correlated in the NIR wave-bands. We perform a Spearman correlation test between the twist and the deviation in ellipticity ($\Delta\epsilon$) for the entire sample of elliptical galaxies. The test result (correlation coefficient -0.35 and probability 0.05) indicates a significant anti-correlation between $\Delta\Phi$ and $\Delta\epsilon$ (see Fig. 18). Note that in the test, a small value of the probability with a negative coefficient suggests significant anti-correlation.

To check whether this result is due to any methodological artifact or indicates a physical effect, we rerun the test two more times with different numbers of galaxies in the elliptical sample. For the first run, we construct the sample after removing only galaxy 10 from group 1. This galaxy shows the largest twist ($\Delta\Phi \sim 68.5^\circ$) in the entire sample and, therefore, we discard it as an outlier. We find that the removal of this galaxy slightly weakens the result (correlation coefficient -0.34 and probability 0.06) but the correlation still remains significant. In the next run, we remove nine galaxies from the entire sample: the first eight galaxies from group 1 because of their spherical shapes ($\epsilon \sim 0.1$) and galaxy 10. This time the test result gives correlation coefficient -0.37 and probability 0.09. Although a greater probability indicates less confidence for this subsample, the result does not differ substantially from the original sample. It suggests that the anti-correlation is a physical effect rather than a fluke.

The NIR correlation between $\Delta\Phi$ and $\Delta\epsilon$ for elliptical galaxies is similar to that in the optical wavelengths. For elliptical galaxies in visual bands, it has been known for a while that the maximum apparent flattening and the maximum observed twist are inversely related (Galletta 1980). An interesting aspect of this correlation would be the possible coupling between NIR and optical light (Jarrett et al. 2003).

Elliptical galaxies with $\epsilon < 0.2$ usually show large variation in their orientations. These galaxies also show considerable differences both in ellipticity and orientation in different bands. The large twist observed in these galaxies should be taken with caution since spherical contours obtained from nearly spherical galaxies are highly prone to spurious effects such as background noise.

The NIR lenticular galaxies have properties similar to those of ellipticals or disk galaxies. The profiles of a few of these galaxies show trends similar to ellipticals. A few of these galaxies show characteristic properties resembling to the galaxies with bar like structures. The lenticular galaxies in our sample, in general, have larger scatter in both ϵ and Φ than the ellipticals. In the entire sample of lenticulars, at least 2 galaxies have bar like signatures in their profiles. The observed twists in the lenticulars' orientations are com-

parable to the trend noticed in spherical galaxies ($\epsilon < 0.2$). The properties of these galaxies stress the fact that morphological classification strongly depends on the wavelength studied. It may be possible that S0 galaxies do not exist in the long wavelength part of the spectrum. This is simply our speculation and more elaborate studies are needed to make this a definite conclusion.

The sample of spiral galaxies indicates that a bar like feature is ubiquitous in disk galaxies without any significant dependence on Hubble's class. This sample has 64 galaxies, of which 24 ($\sim 38\%$) are optically-classified barred galaxies. Most of these galaxies show features resembling bar(s) in the infrared. We label these galaxies as "optical and infrared bar" ("OIB"). However, we notice something interesting. All most one-third of these optical barred galaxies lack characteristic features in their NIR profiles. These galaxies include: NGC 4394(12) in group 1 (Fig. 10); NGC 4375(6) and UGC 7073(9) in group 3 (Fig. 14); UGC 2705(4), UGC 3171(9), NGC 5510(13), and UGC 1478(16) in group 4 (Fig. 16).

The sample of spirals include 40 galaxies that are optically classified non-barred galaxies. At least 11 of these galaxies show bar like features in their NIR profiles, increasing the number of bar like systems to $\sim 45\%$. Several previous studies have also reported a higher frequency of barred systems in disk galaxies (Seiger & James 1998; Eskridge et al. 2000; Laurikainen & Salo 2002). Our result is in agreement with all of these studies except Seiger & James (1998), who reported $\sim 90\%$ frequency of barred galaxies from a sample of 45 spirals imaged in NIR J and K bands. Our estimate indicates that a significant fraction of disk galaxies are intrinsically non-barred systems. The absence of a bar like feature in the profiles of 29 spiral galaxies favors this argument. This is also consistent with Eskridge et al. (2000).

Among 19 normal spiral galaxies, 17 galaxies are SA-type. The other two, UGC 5739 in group 1 and IC 2947 in group 3, are irregular/peculiar type galaxies. In these 17 SA-type spirals, 5 galaxies have distinct bar like features in their shape profiles indicating that $\sim 30\%$ of SA-type galaxies have optically hidden bars. Our result is in agreement with Eskridge et al. (2000) who reported $\sim 40\%$ galaxies have optically hidden bars from a sample of 186 NIR H -band spirals containing 51 non-barred SA-type galaxies.

Note that several disk galaxies show multiple bar features in their profiles. However, in this study we only report their morphologies and do not attempt to make any definite conclusion regarding their projected structure since identifying galaxies with multiple bars is a complicated issue (see Wozniak et al. 1995; Erwin & Sparke 1999). It is important to note that our estimate of the frequency of barred galaxies is done by visual inspection. Since the sample of galaxies used in this study is not based on rigorous selection criteria, the results should be taken as an approximate estimate.

The overall isophotal twists observed in the orientations of spiral galaxies range between $\sim 3^\circ - 71^\circ$. Many NIR barred spirals appear to have smaller but notable twists in their orientations than the twist at optical wavelengths (see e. g., Wozniak et al. 1995). Two conclusions can be drawn after analyzing the orientation profiles of the NIR images. First, the NIR light in J , H , and K_s bands is not fully decoupled from Population I light. They are most likely weakly coupled. Second, the different regions (central bulge, bar,

and outer disk) of disk galaxies are dynamically linked. It is manifested in the continuous change in the orientations of the majority of the disk galaxies. Exceptions are noticed in few cases, e. g., NGC 3384 (10, group 1; Fig. 11), NGC 4152 (4, group 2; Fig. 13), UGC 2303 (1, group 3; Fig. 15), where the change in the orientation is very sharp. But it is important to note that in the region where the sharp changes are observed, the galaxy contours appear to be very spherical ($\epsilon \leq 0.15$). A drastic change in the orientations of spherical contours does not indicate reliably the actual nature of the internal structure since these types of contours are prone to spurious effects.

Acknowledgments We thank the referee for his constructive criticisms and many helpful suggestions. We are indebted to Bruce Twarog for thorough and critical reading of the manuscript. His suggestions improved the paper significantly. NR thanks Tom Jarrett, Hume Feldman, and Barbara Anthony-Twarog for useful discussions. NR acknowledges the GRF support from the University of Kansas in 2002-2003. SFS acknowledges the support from the Nonlinear Cosmology Program, 2003 at Observatory de la Cote d'Azur in Nice, France during the summer 2003 and the AAS travel grant.

This research has made use of the NASA/IPAC Infrared Science Archive, which is operated by the Jet Propulsion Laboratory, California Institute of Technology, under contract with the National Aeronautics and Space Administration.

6 APPENDIX

Here we briefly describe the role of contour smoothing in our analyses. We also discuss the sensitivity of the parameters to any disturbance present on the contour.

In order to emphasize the role of contour smoothing we show in Fig. 19 the ellipticity measured from all three AEs, both for unsmoothed and smoothed elliptical galaxies in group 1. In this figure the dark, medium, and light colors are used to represent the J , H , and K_s band respectively. The solid, dashed, and dashed-dotted lines show the area, perimeter, and EC ellipses for each band. As we can see from the unsmoothed contours in the left panel, the ellipses differ from one another in each band mostly near the edge. This deviation is caused by the background noise since the galaxy surface brightness distribution is steeper near the center and shallower outward. We should also note that in a region far away from the center of a galaxy the absolute value of the distribution is very small. In either case any kind of background noise will have a strong effect on the outer part of the distribution. Therefore when one constructs contours along the edge of a galaxy, they appear highly deviated no matter what their true shapes are. If the contours were truly elliptical, they could appear in any arbitrary shape depending on the amount distortion. Since the contours are not elliptic anymore, the AEs diverge from one another. This divergence reflects the apparent shape of the contours. One can see from the right panel that contour smoothing reduces the role of noise significantly. It helps restore the original shape of the contours. At the same time one can also notice that the differences among the ellipses reduce substantially. To

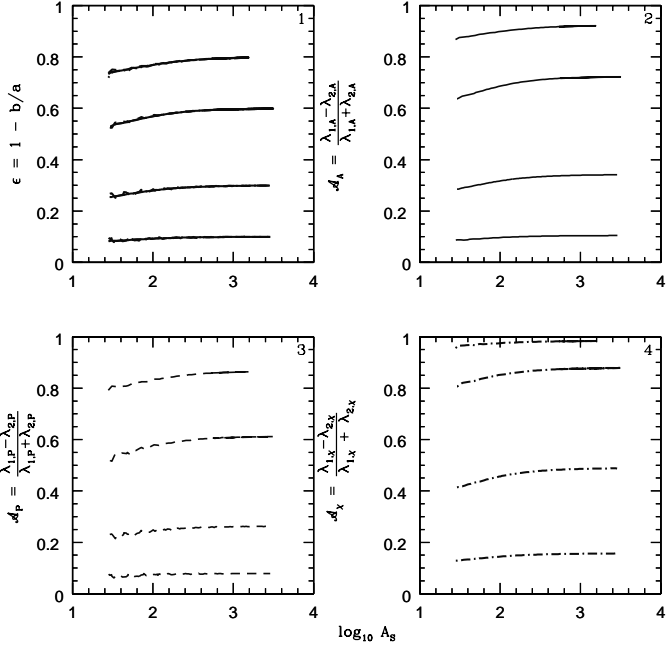


Figure 1. Ellipticity (ϵ_i) and Anisotropy (A_i) as a function of contour area (A_S) for various elliptical profiles. For each profile, panel 1 have ϵ_i of three AEs whereas panels 2, 3, and 4 show, respectively, A_A , A_P , and A_X . In the figure solid, dashed and dashed-dotted lines represent, respectively, the parameters derived from the area, perimeter, and EC tensor. For perfect elliptical profiles, the lines showing ϵ_i stay on top of each other giving the identical result. The AEs behave similarly for elliptical profiles of arbitrary flattening. The A_i , however, do not coincide. The relative separations between the lines representing different tensors change with the flattening of the profiles. Note that for highly flattened systems central regions appear less elongated due to discreteness effect.

demonstrate further, we collect first four galaxies from each group of spiral galaxies and show the ellipticity for both unsmoothed and smoothed contours in Figs. 20 and 21, respectively. The motive, once again, is to reemphasize the role of contour smoothing.

When we compare Figs. 19 and 21, it appears that the color difference is, in general, stronger for spiral galaxies and within spirals, it is stronger for certain Hubble types. We see that the galaxies in spiral group 4, which are mostly late-type, have significant differences in their shapes (at least what is revealed by the ϵ parameter) when studied in three different NIR bands.

We now proceed to check the sensitivity of the Minkowski shape measures to detect image contamination by a foreground star. The J band contours of NGC 4278, NGC 3193, NGC 3379 (1, 4, and 7 in elliptical group 1), are shown in Fig. 22. This figure also includes the contours of NGC 5507 (5 in elliptical group 2) from the same band. Note that the presence of a star is apparent in all three bands. It is most prominent in the J band and this why we show the contour plot in this band.

The left panel of Fig. 23 shows the ellipticity profiles of these galaxies and the right panel shows the relative difference in areas enclosed by three tensor AEs. In the left panel

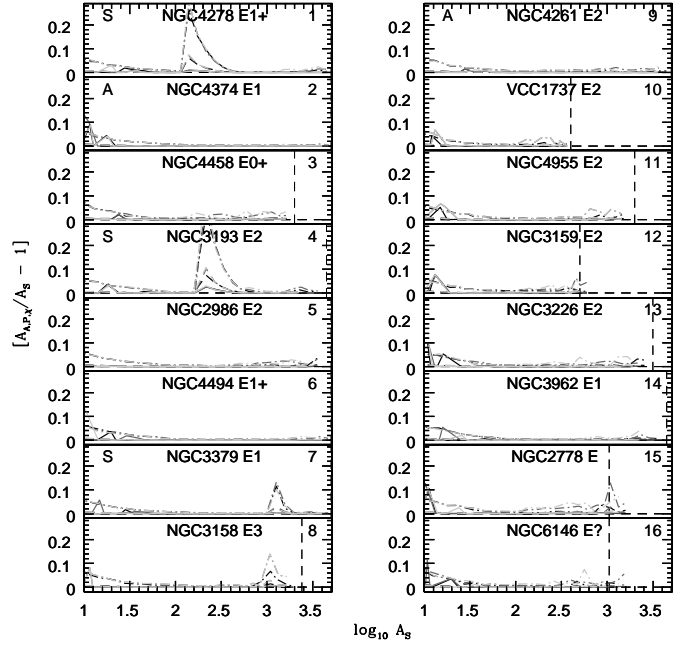


Figure 2. The relative difference in the areas enclosed by three different AEs as a function of contour area (A_S) for a selection of elliptical galaxies. Each panel contains a total of nine curves : three curves corresponding to three AEs at each band. The dark, medium and light colors to represent J , H , and K_s band, respectively. The area, perimeter, and EC ellipses are shown, respectively, by the solid, dotted, and dashed-dotted lines. The vertical dashed line represents the area within the contour that corresponds to K_s band $3 \times \sigma_n$ isophotal region. For some galaxies this line goes beyond the horizontal range shown above. The number 1 to 16 shown at top-right in each panel is used just to label the galaxies.

we use solid, dashed and dashed-dotted lines represent the measures from area, perimeter and EC AEs. The dotted line is the measure from the scalar functional AE that has not been used in this analysis. It is included only for the purpose of illustration. Note that the construction of the scalar ellipse is different from the tensor ellipses. Since the scalar functionals are simply the area (A_S) and perimeter (P_S) of a given contour, the scalar AE is an ellipse that has the same area and perimeter as the contour itself. For a perfect elliptical contour, the scalar AE will converge with its tensor counterparts. The scalar functionals do not have enough information to attribute an orientation to its ellipse. The right panel does not show any measurement from the scalar functional.

From Figs. 22 and 23, we see that a foreground star embedded in an image causes galaxy isophotes to deviate from their original shapes. It usually adds small, lobe-like features to the otherwise smoothed and spherical contours. The functionals easily pick up this type of signal present on the contour and translate it to the shape parameters. This demonstration highlights the fact that MFs based measures can be used for automatic detection of features attached to the image body.

Our analysis is further supported by NGC 5077 (num-

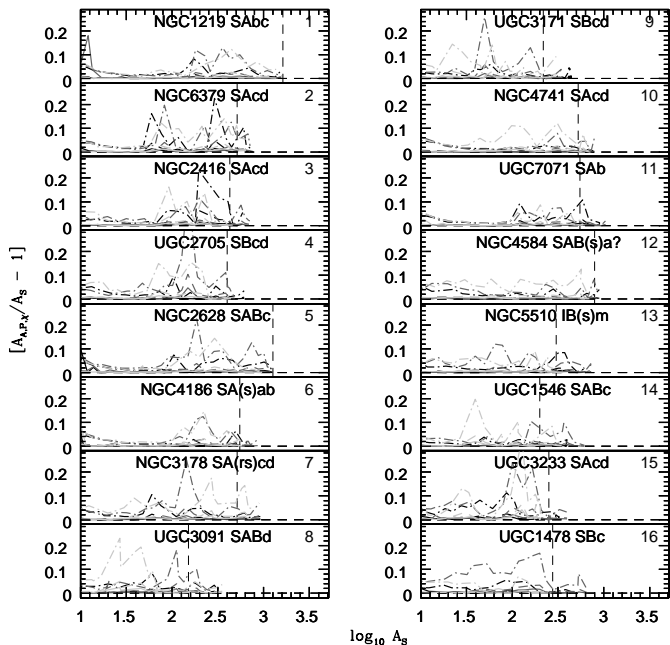


Figure 3. The relative difference in the areas enclosed by different AEs as a function of contour area (A_S) for a selection of spiral galaxies. The line styles and colors are similar to Fig. 2.

ber 5 in elliptical group 2). This galaxy is interesting for our purpose since it has been archived in the 2MASS catalogue as an image free from foreground star. The contour plot of the galaxy, however, reveals that it is not the case since the isophotal contours are perturbed by an uncommon feature. Apart from the contour plot, the behavior of the ellipticity profile or the plot showing ratios of the sizes of AEs also give strong indication of the presence of something unusual in the image body. From the extent of the feature along the radial direction one can infer the possible nature of the object that distorts the image contours. A close inspection of the contours and a comparison with the other galaxies mentioned above lead us to conclude that a foreground star is still left embedded in the galaxy image.

With these examples at hand, we feel confident to suggest that both ellipticity and the ratios of the sizes of AEs can be used simultaneously as filtering tools in image processing. These measures may appear useful to reduce the chance of contamination by foreground star while constructing large galaxy catalogues from surveys such as Sloan Digital Sky Survey (SDSS).

REFERENCES

- Abraham R. G., Merrifield M. R., Ellis R. S., Tanvir N. R., Brinchmann J., 1999, MNRAS, 308, 569
 Abraham R. G., Merrifield M. R., 2000, ApJ, 120, 2835
 Athanassoula E., Morin S., Wozniak H., Puy D., Pierce M. J., Lombard J., Bosma A., 1990, MNRAS, 245, 130
 Bender R., Möllenhoff C., 1987, A&A, 177, 71
 Beisbart C., 2000, Ph.D. Thesis, Ludwig-Maximilians-Universität, München, Germany
 Beisbart C., Buchert T., Wagner H., 2001a, Physica A, 293, 592B

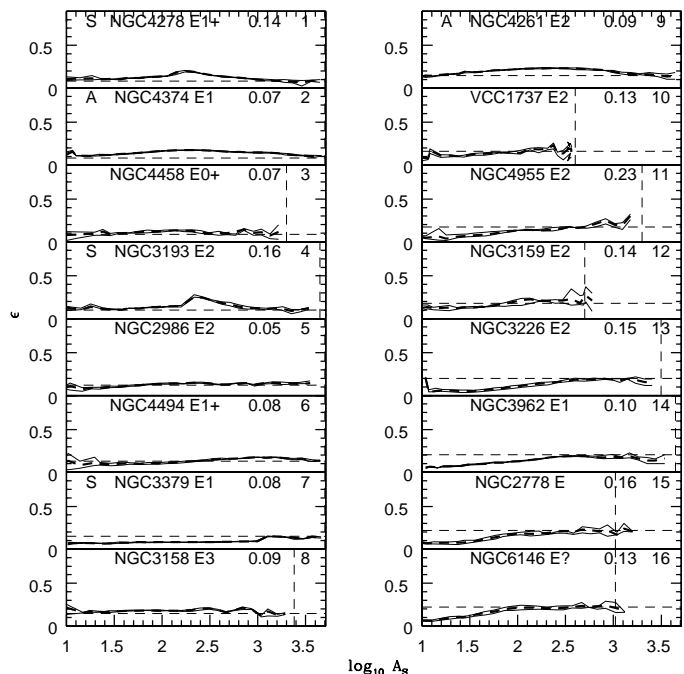


Figure 4. Ellipticity as a function of contour area (A_S) for elliptical galaxies in group 1 (2MASS $\epsilon \leq 0.2$). The thick dashed line represents the mean ellipticity of three different NIR bands: J , H , and K_s . The upper and lower thin solid lines are used to show the maximum and minimum ellipticity measured in these three bands. The horizontal and vertical dashed lines represent, respectively, the 2MASS estimate of K_s band $3 \times \sigma_n$ isophote ellipticity and the area within the contour corresponding to that isophote. Note that for some galaxies the vertical line goes beyond the horizontal range of the figure. The NED galaxy name, its RC3 classification, and the overall deviation ($\Delta\epsilon$) in ellipticity are shown at the top of each panel. The difference between the highest and lowest value of the thick dashed line, in the range $\log_{10} A_S \geq 1.5$, is used to measure $\Delta\epsilon$. Similar style is followed for the rest of the presentation. For the meaning of the symbols “A” and “S” see text.

- Beisbart C., Valdarnini R., Buchert T., 2001b, A&A, 379, 412
 Buta R., Block D. L., 2001, ApJ, 550, 243
 Carter D., 1978, MNRAS, 182, 797
 Carter D., Metcalfe N., 1980, MNRAS, 191, 325
 de Vaucouleurs G., de Vaucouleurs A., Corwin H. G. Jr., Buta R., Paturel G., Fouqué P., 1991, Third Reference Catalogue of Bright Galaxies (Berlin: Springer) (RC3)
 Eskridge P. B. et al., 2000, AJ, 119, 536
 Erwin P., Sparke L. S., 1999, ApJ, 521, L37
 Erwin P., Sparke L. S., 2003, ApJSS, 146, 299
 Fasano G., Bonoli C., 1989, A&ASS, 79, 291
 Franx M., Illingworth G., Heckman T., 1989, AJ, 98, 538
 Galletta G., 1980, A&A, 81, 179
 Hobson M. P., Jones A. W., Lasenby A. N., 1999, MNRAS, 309, 125
 Jarrett T. H., 2000, PASP, 112, 1008
 Jarrett T. H., Chester T., Cutri R., Schneider S., Skrutskie R., Huchra J. P., 2000, ApJ, 119, 2498
 Jarrett T. H., Chester T., Cutri R., Schneider S., Skrutskie R., Huchra J. P., 2003, AJ, 125, 525
 Jędrzejewski R. I., 1987, in Structure and Dynamics of Elliptical Galaxies, ed. T. de Zeeuw, (Dordrecht: Reidel), p. 37

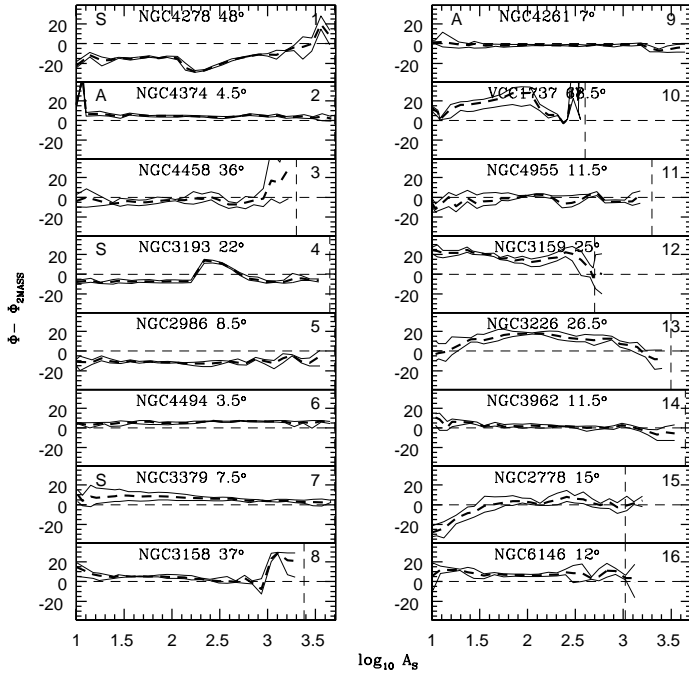


Figure 5. Orientations (in degrees) of elliptical galaxies in group 1 ($2MASS \epsilon \leq 0.2$) presented with respect to the $2MASS K_s$ band $3 \times \sigma_n$ isophote position angle. The NED galaxy name and the overall twist ($\Delta\Phi$) in the orientation of galaxies are shown at the top of each panel. The difference between the highest and lowest value of the thick dashed line, in the range, $\log_{10} A_S \geq 1.5$, is used to estimate $\Delta\Phi$.

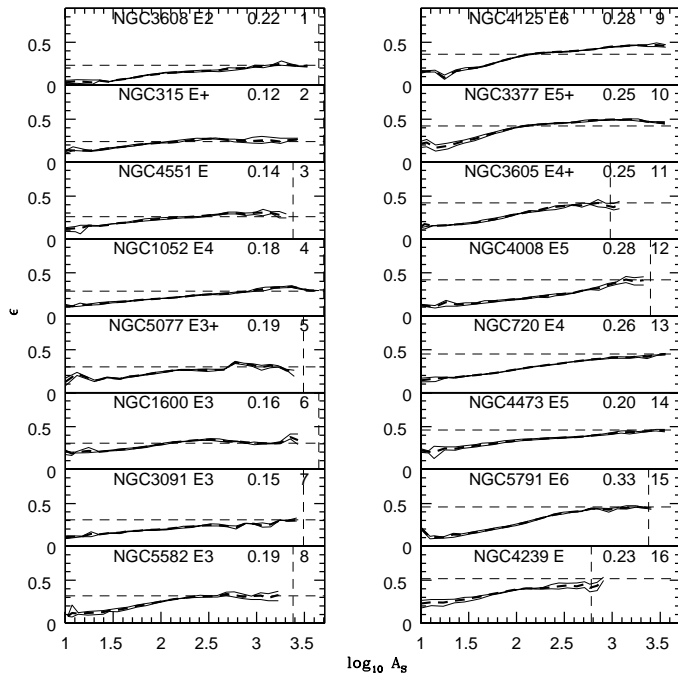


Figure 6. Ellipticity as a function of contour area (A_S) for elliptical galaxies in group 2 ($2MASS \epsilon > 0.2$).

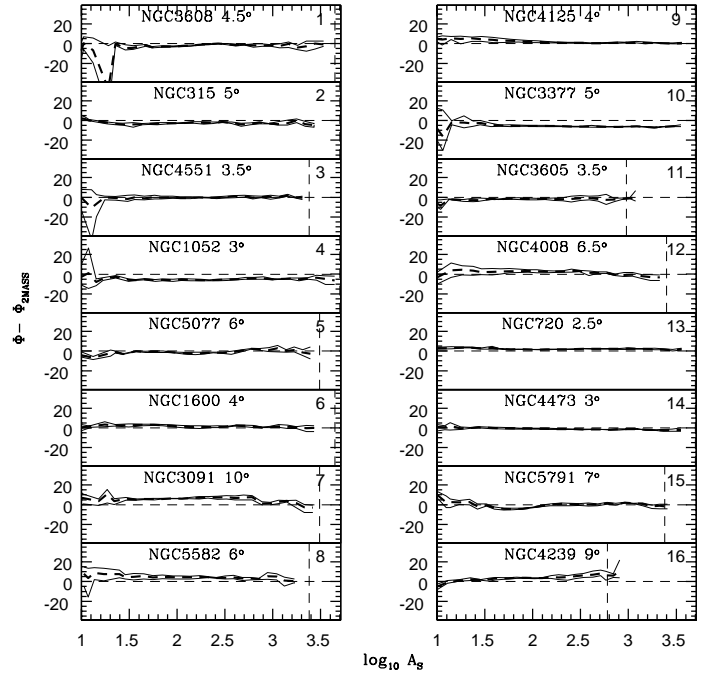


Figure 7. The orientations of elliptical galaxies in group 2 ($2MASS \epsilon > 0.2$).

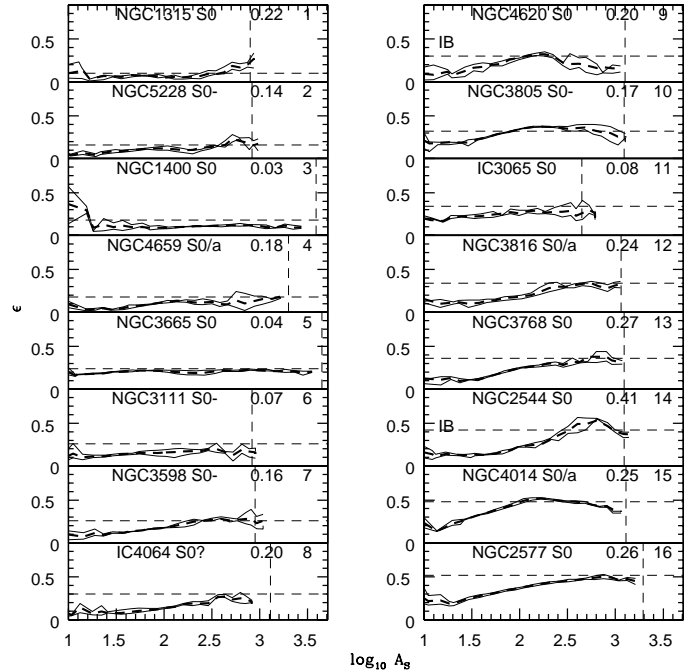


Figure 8. Ellipticity as a function of contour area (A_S) for lenticular galaxies. The label “IB” is used to represent the galaxy that has bar like feature only in the infrared.

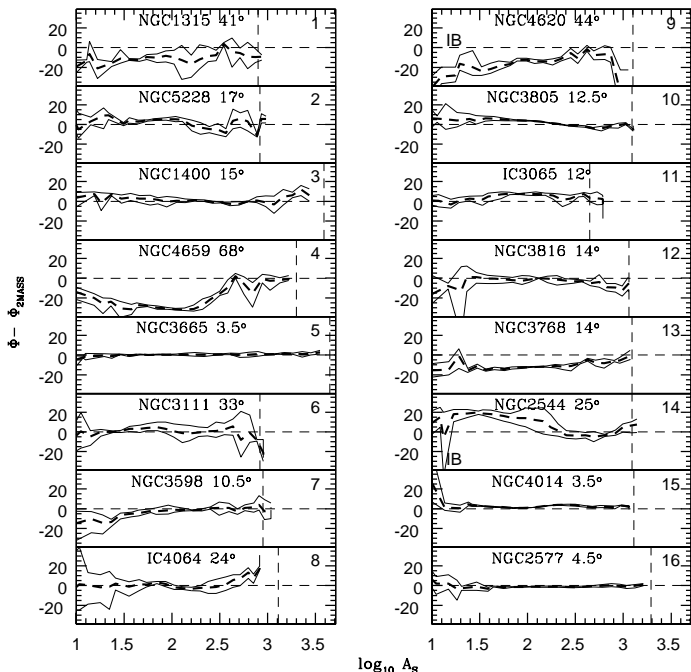


Figure 9. Orientations of lenticular galaxies shown in Fig. 8. The label “IB” is used to represent the galaxy that has a bar like feature only in the infrared. The profiles of galaxy 1 and 4 are scaled by a factor 2 to fit the range along the vertical axis. No scaling is applied to the other galaxies.

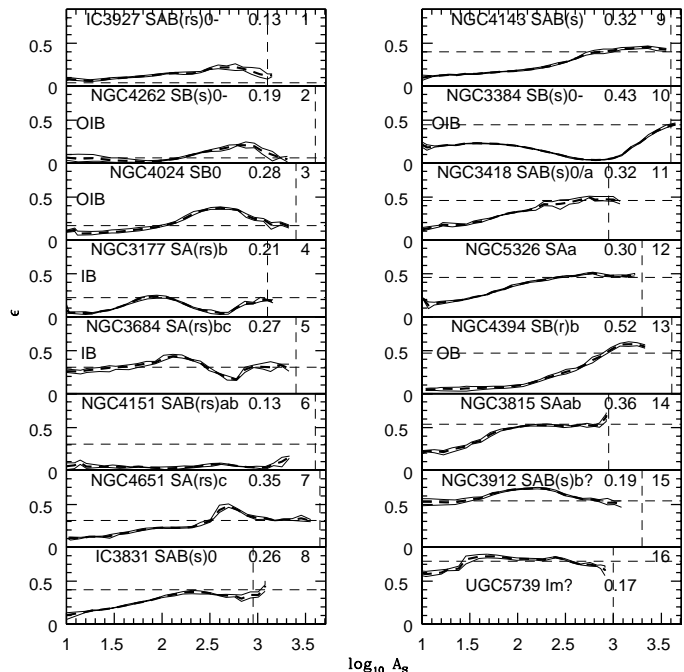


Figure 10. Ellipticity as a function of contour area (A_S) for spiral galaxies in group 1. The labels “OIB” and “OB” represent, respectively, “optical and infrared bar” and “optical bar”. Note that the spiral galaxies are divided into four groups. The groups are organized using the scatter ($\delta\epsilon$) observed on the ellipticity profiles. The galaxies in spiral group 1 have the least scatter ($\delta\epsilon \leq 0.05$).

Kerscher M. et al., 1997, MNRAS, 284, 73
 Kerscher M., Mecke K., Schmalzing J., Beisbart C., Buchert T., Wagner H., 2001a, A&A, 373, 1
 Kerscher M. et al., 2001b, A&A, 377, 1
 Leach R., 1981, ApJ, 248, 485
 Lauer T., 1985, MNRAS, 216, 429
 Laurikainen E., Salo H., Rautiainen P., 2002, MNRAS, 331, 880
 Laurikainen E., Salo H., 2002, MNRAS, 337, 1118
 Michel-Dansac L., Wozniak H., 2004, A&A, 421, 863
 Martin P., 1995, AJ, 109, 2428
 Mecke K. R., Buchert T., Wagner H., 1994, A&A, 288, 697
 Minkowski H., 1903, Math. Ann., 57, 447
 Novikov D., Feldman H. A., Shandarin S. F., 1999, Int. J. Mod. Phys., D8, 291
 Novikov D., Schmalzing J., Mukhanov V. F., 2000, A&A, 364, 17
 Peletier, R. F., Davis, R. L., Illingworth, G. D., Davis, L. E., Cawson M., 1990, AJ, 100, 1091
 Quillen A. C., Frogel J. A., Gonzalez R. A., ApJ, 1994, 437, 162
 Rahman N., Shandarin S. F., 2003, MNRAS, 343, 933 (paper I)
 Rozas M., Knapen J. H., Beckman J. E., 1998, MNRAS, 301, 631
 Sahni V., Sathyaprakash B. S., Shandarin S. F., 1998, ApJ, 495, L5
 Schmalzing J., Buchert T., 1997, ApJ, 482, L1
 Schmalzing J., Gorski K. M., 1998, MNRAS, 297, 355
 Schmalzing J., Buchert T., Melott A. L., Sahni V., Sathyaprakash B. S., Shandarin S. F., 1999, ApJ, 526, 568
 Seigar M. S., James P. A., 1998, MNRAS, 299, 672
 Shandarin S. F., 2002, MNRAS, 331, 865
 Shandarin S. F., Feldman H. A., Xu Y., Tegmark M., 2002, ApJS, 141, 1
 Sheth J., Sahni V., Shandarin S. F., Sathyaprakash B. S., 2003, MNRAS, 343, 22S
 Williams T. B., Schwarzschild M., 1979, ApJ, 227, 56

Wozniak H., Pierce M. J., 1991, A&AS, 88, 325
 Wozniak H., Friedli D., Martinet L., Martin P., Bratschi P., 1995, A&ASS, 111, 115

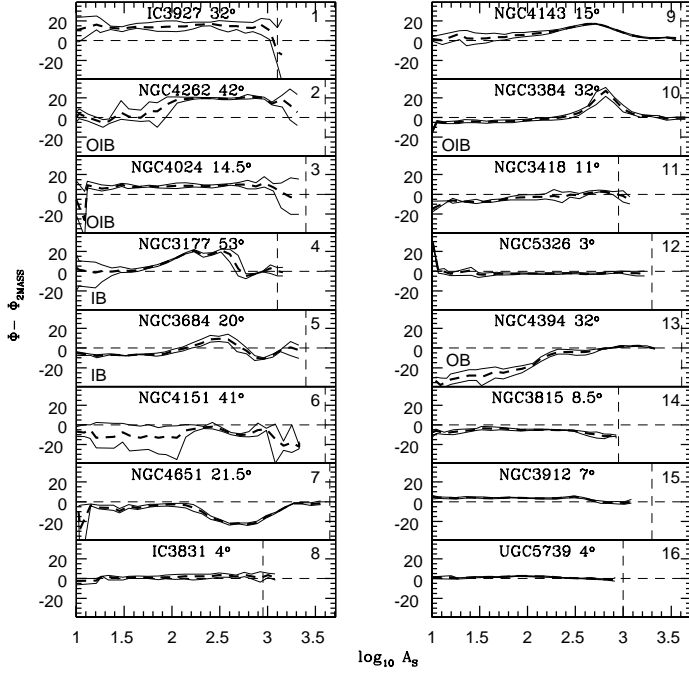


Figure 11. Orientations of galaxies in spiral group 1. Galaxies, numbered as 2, 4, and 6, are scaled by a factor 2 to fit the range along the vertical axis. No scaling is applied to other galaxies.

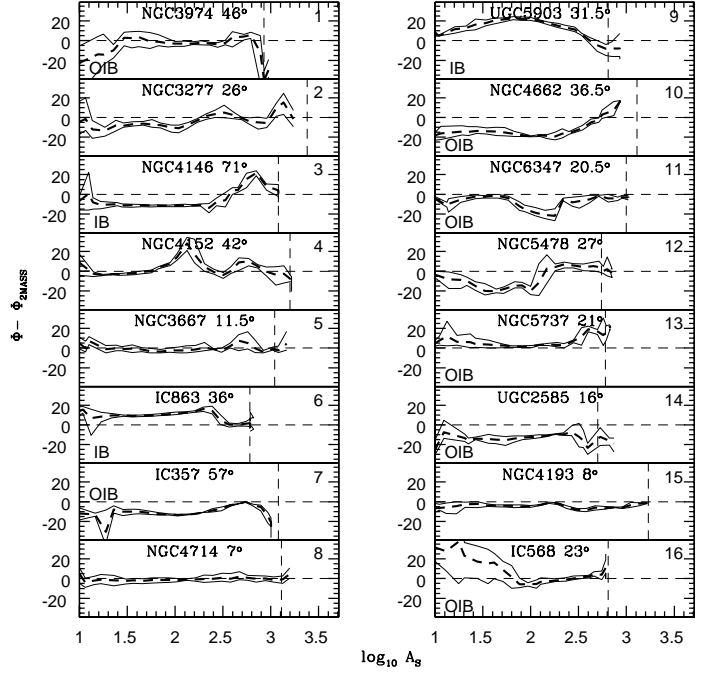


Figure 13. Orientations of galaxies in spiral group 2. Galaxies, numbered as 3, 6, and 7, are scaled by a factor 2 to fit the range along the vertical axis. No scaling is applied to other galaxies.

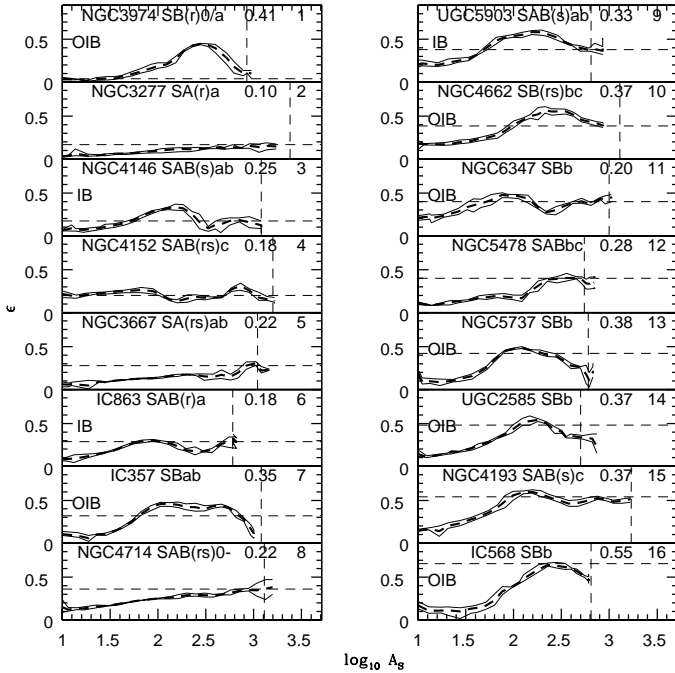


Figure 12. Ellipticity as a function of contour area (A_s) for spiral galaxies in group 2. The galaxies have scatter in ellipticity in the range $0.05 < \delta\epsilon \leq 0.1$ when J , H , and K_s band measurements are compared.

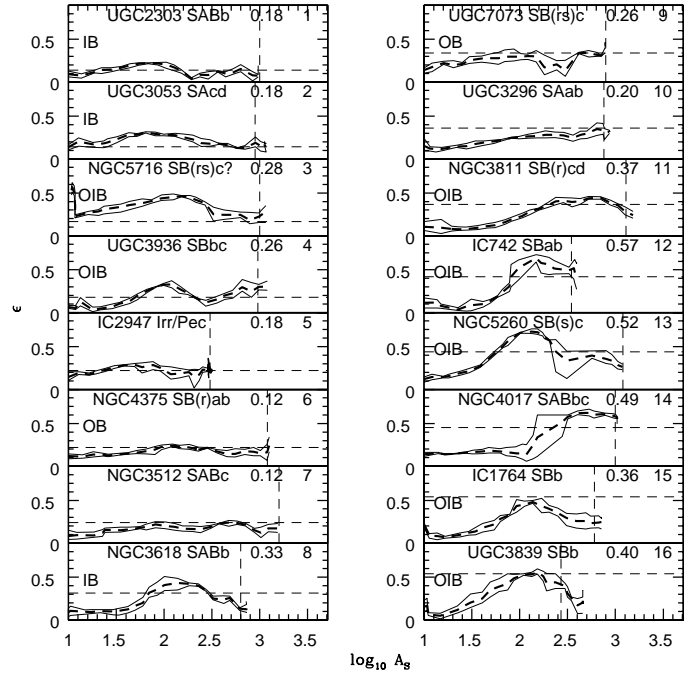


Figure 14. Ellipticity as a function of contour area (A_s) for spiral galaxies in group 3. The galaxies have scatter in the range, $0.1 < \delta\epsilon \leq 0.2$, in J , H , and K_s band measurements. Note that NGC 4375(6), an optical barred system (“OB”) lacks characteristic feature in its NIR profile.

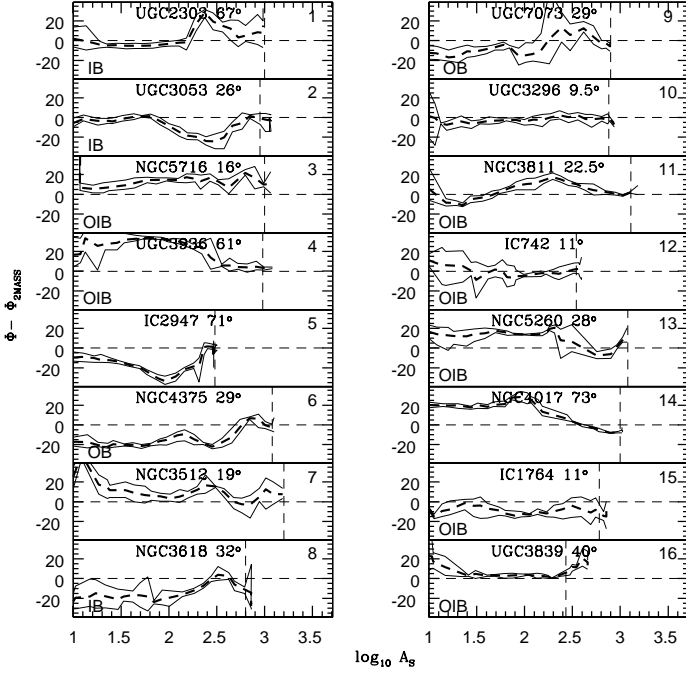


Figure 15. Orientations of galaxies in spiral group 3. Galaxies, numbered as 1, 4, 5, 14, and 16, are scaled by a factor 2 to fit the range along the vertical axis. No scaling is applied to other galaxies.

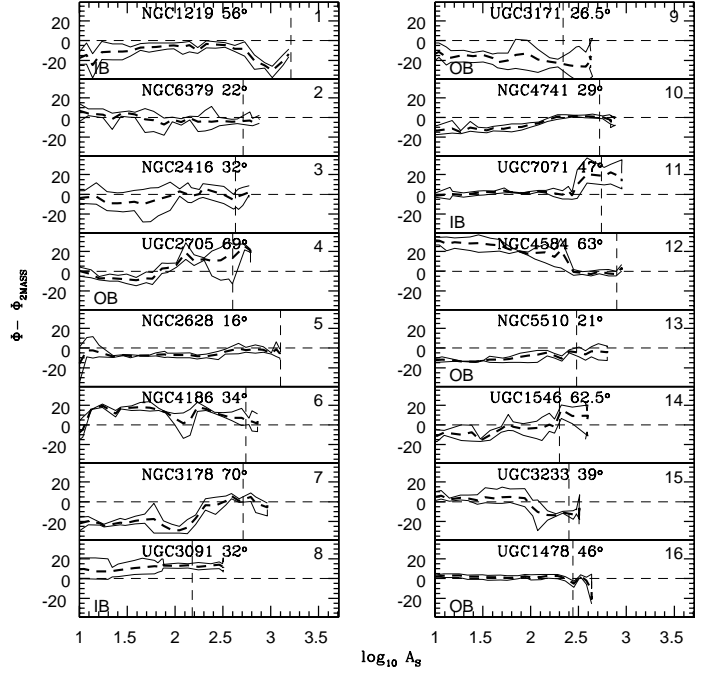


Figure 17. Orientations of galaxies in spiral group 4. Galaxy UGC 3091(8) is scaled by a factor 4 to fit the range along the vertical axis. The other galaxies are scaled by a factor 2.

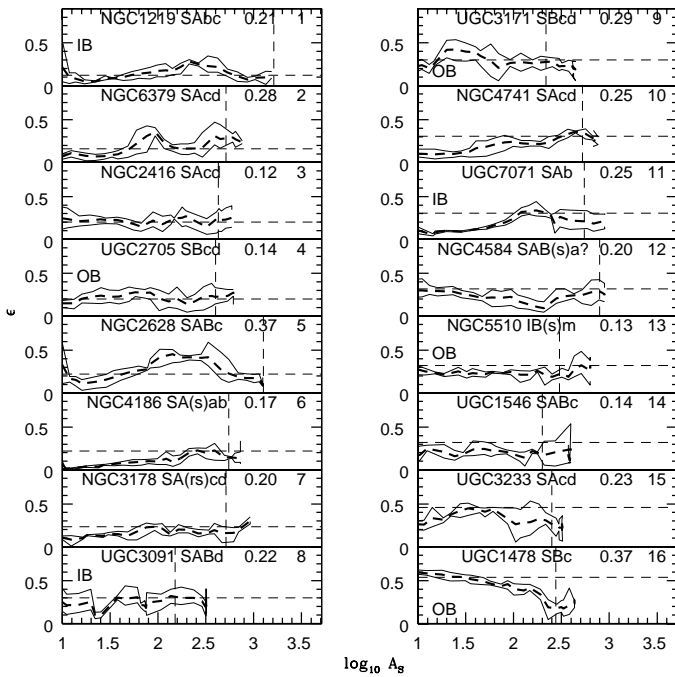


Figure 16. Ellipticity as a function of contour area (A_S) for spiral galaxies in group 4. The galaxies have scatter $\delta\epsilon > 0.2$ in J , H , and K_s band measurements.

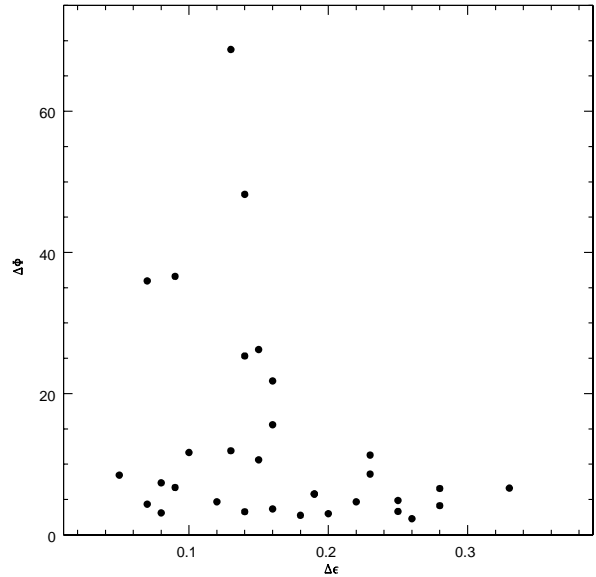


Figure 18. Twist ($\Delta\Phi$, in degree) versus deviation in ellipticity ($\Delta\epsilon$) for the entire sample of elliptical galaxies. The Spearman correlation test, with a correlation coefficient of -0.35 and a probability of 0.05, indicates a significant anti-correlation between these two parameters.

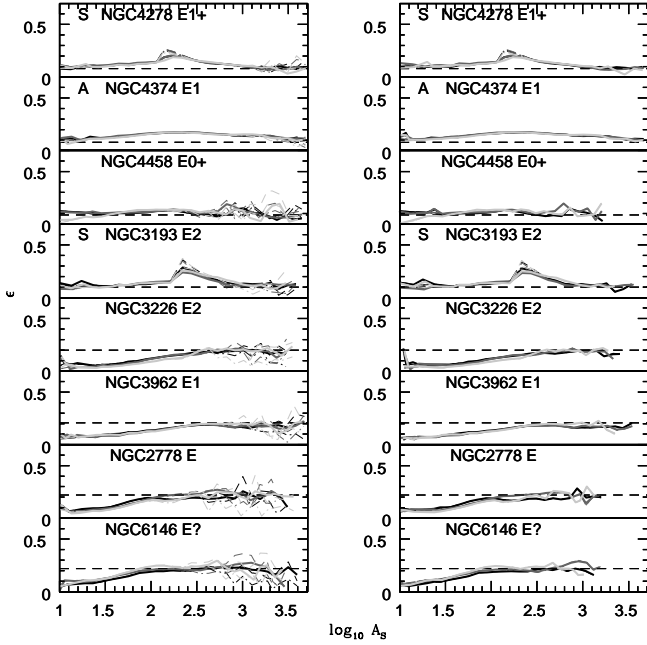


Figure 19. Ellipticity as a function of area (A_S) obtained from unsmoothed (left panels) and smoothed (right panels) contours of a selection of elliptical galaxies from group 1. The dark, medium, and light colors show the measurements from J , H , and K_s bands respectively. For each band the solid, dashed and dashed-dotted lines represent the ellipticity measure of the area, perimeter and EC AEs. The symbols “A” and “S” are explained in the text. Notice how contour smoothing reduces the effect of noise, retaining the main features of the contours; different AEs for each band converge and stay on top of each other. The convergence indicates that the galaxy contours are indeed elliptical in nature, revealed by smoothing.

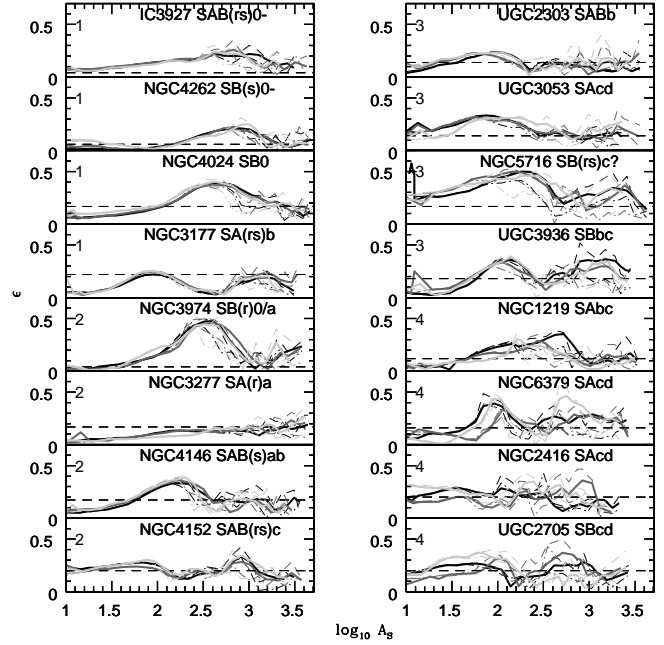


Figure 20. Ellipticity as a function of area (A_S) obtained from unsmoothed contours of spiral galaxies. The first four galaxies from each spiral group are shown in this figure marked by numbers 1 to 4, where 1 stands for group 1 and so on. The line styles and colors are similar to Fig. 19.

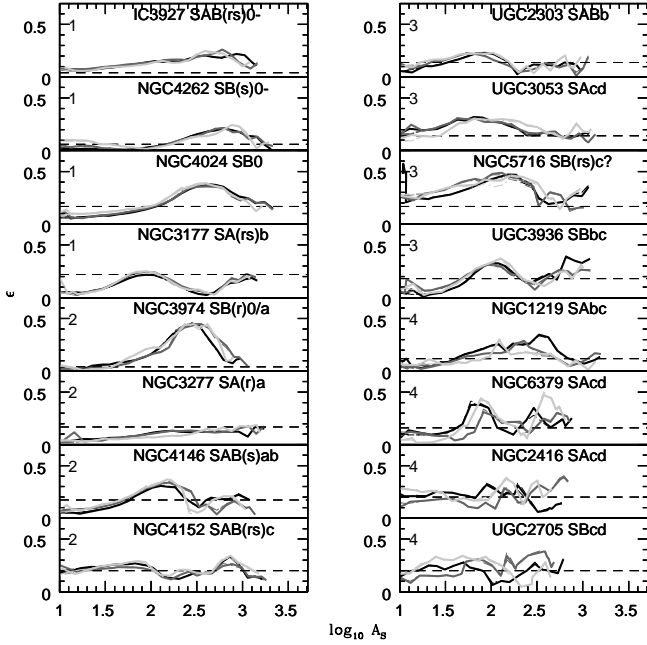


Figure 21. Ellipticity as a function of area (A_S) for smoothed contours of spiral galaxies in Fig. 20. The line styles and colors are the same as before. The convergence of the AEs is a result of smoothing and illustrates the fact that the contours of the spiral galaxies are elliptic in nature although the ellipticity varies with image size. In comparison to Fig. 20, one can see that contour smoothing reduces noise, keeping the main features intact. One can also notice that the color difference is stronger in late type spirals (lower four panels on the right, marked with the number 4).

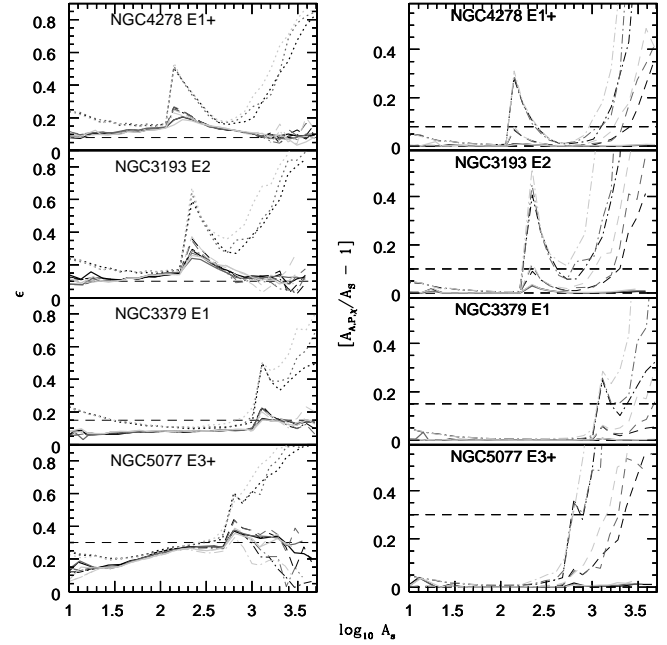


Figure 23. Ellipticity (left panel) and relative differences in the areas enclosed by different AEs (right panel) for elliptical galaxies where a foreground star is embedded in the galaxy images. The figure shows information from all three bands. Dark, medium, and gray colors represent, respectively, the J , H , and K_s band. The dotted line represents ellipticity from the scalar functional (see appendix for more); the solid, dashed, and dashed-dotted line represent the ellipticities of the area, perimeter, and EC AEs, respectively. A sharp kink in the ellipticity profiles is the signature of the embedded foreground star. A similar feature can also be seen from the plot showing the ratios of the sizes of AEs.

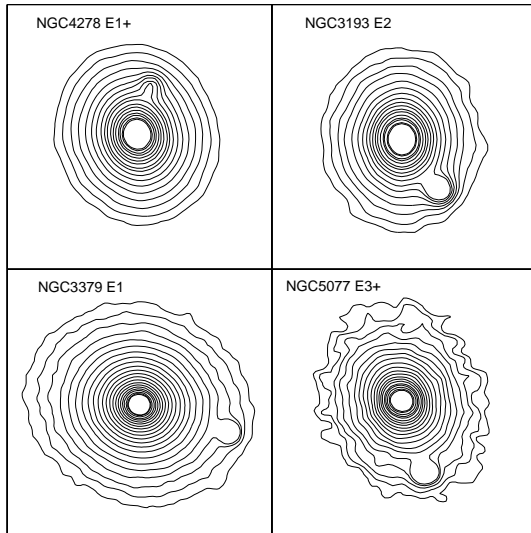


Figure 22. The unsmoothed contour plot of galaxies in J band. In each of these galaxy images a foreground star is left embedded. The presence of the lobe-like feature on contours is a signature of embedded foreground star.